Supplement of The Cryosphere, 18, 2081–2101, 2024
https://doi.org/10.5194/tc-18-2081-2024-supplement

The Cryosphere Open Access EGU

Supplement of

Towards the systematic reconnaissance of seismic signals from glaciers and ice sheets – Part 2: Unsupervised learning for source process characterization

Rebecca B. Latto et al.

Correspondence to: Rebecca B. Latto (beccablatto@gmail.com)

Table of Contents

Supplementary files related to material presented in the main text are publicly available in https://github.com/beccalatto/multi_sta_lta/unsupervised_learning_for_cryoseismology/.
File names and description are listed below.

TraceFeatureDatasetWhillans.csv : Trace feature dataset for the Whillans Ice Stream

ReferenceFeatureDatasetWhillans.csv : Reference feature dataset for the Whillans Ice Stream

ReferenceClusterLabelsWhillans_k10.csv : Reference event catalogue with reference features and a column for the cluster label from k-means++ applied to data from the Whillans Ice Stream, for k=10

Table S1: Overview of features and transformations. Provided are the method of computation for each reference feature, in terms of log or linear scaling applied to the feature derived from the top three seismometers or similar (middle column) and traces used in feature calculation (right column). First, the energy of each trace is calculated as an integral of the trace. Then, each reference feature per event is calculated from the three seismometers with the highest energy detections of the event that detected that event such that the reference feature best characterizes the event's corresponding waveform.

Feature description [tag]	**Log or linear**	**Trace(s) used in feature calculation**
Number of stations that detect an event [0]	Linear	All
Duration [1]	Log	Reference event catalogue (handles travel time)
Ratio of the mean over the maximum of the envelop signal [2]	Linear	Median of the 3 most energetic traces
Ratio of the median over the maximum of the envelop signal [3]	Linear	Median of the 3 most energetic traces
Ratio between ascending and descending time [4]	Log	Median of the 3 most energetic traces
Kurtosis of the raw signal (peakness of the signal) [5]	Log	Median of the 3 most energetic traces
Kurtosis of the envelop [6]	Log	Median of the 3 most energetic traces
Skewness of the raw signal [7]	Log	Median of the 3 most energetic traces
Skewness of the envelop [8]	Log	Median of the 3 most energetic traces
Energy in the first third part of the autocorrelation function [10]	Log	Median of the 3 most energetic traces
Energy in the remaining part of the autocorrelation function [11]	Log	Median of the 3 most energetic traces
Energy of the signal filtered in 0.001 - 0.03 Hz [13]	Log	2nd most energetic trace in this frequency band
Energy of the signal filtered in 0.01 - 0.3 Hz [14]	Log	2nd most energetic trace in this frequency band
Energy of the signal filtered in 0.1 - 3 Hz [15]	Log	2nd most energetic trace in this frequency band
Energy of the signal filtered in 1 - 30 Hz [16]	Log	2nd most energetic trace in this frequency band
Energy of the signal filtered in 10 - 100 Hz [17]	Log	2nd most energetic trace in this frequency band
Kurtosis of the signal filtered in above 5 frequency bands [18–22]	Log	Median of 3 most energetic traces computed for each frequency band
Mean of the discrete Fourier transform [24]	Log	Median of the 3 most energetic traces
Max of the discrete Fourier transform [25]	Log	Median of the 3 most energetic traces
Central frequency of the 1st quartile [27]	Linear	Median of the 3 most energetic traces
Central frequency of the 2nd quartile [28]	Linear	Median of the 3 most energetic traces
Median of the normalized discrete Fourier transform [29]	Linear	Median of the 3 most energetic traces
Variance of the normalized discrete Fourier transform [30]	Log	Median of the 3 most energetic traces

Energy in [0, 1/4] Nyquist frequency [34]	Log	2nd most energetic trace across spectrum
Energy in [1/4,1/2] Nyquist frequency [35]	Log	2nd most energetic trace across spectrum
Energy in [1/2, 3/4] Nyquist frequency [36]	Log	2nd most energetic trace across spectrum
Energy in [3/4, 1] Nyquist frequency [37]	Log	2nd most energetic trace across spectrum
Spectral centroid [38]	Linear	Median of the 3 most energetic traces
Gyration radius [39]	Linear	Median of the 3 most energetic traces
Spectral centroid width [40]	Linear	Median of the 3 most energetic traces
Rectilinearity [68]	Linear	Median of the 3 most energetic traces
Dip [70]	Linear	Median of the 3 most energetic traces
Planarity [71]	Linear	Median of the 3 most energetic traces

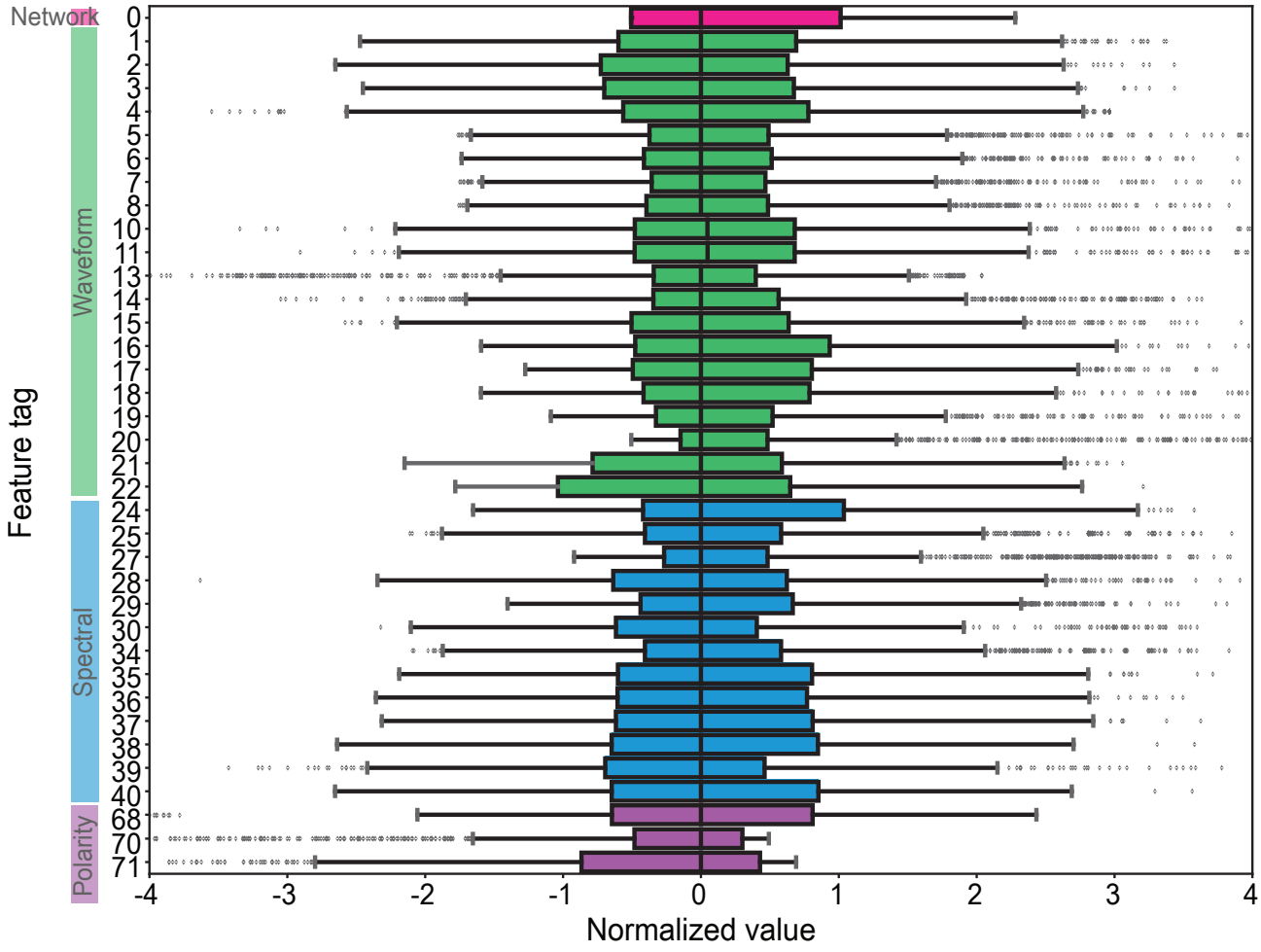

Figure S1. Distribution of each feature in the feature dataset after log or linear scaling and normalization. The feature tags and color attributions (top to bottom: pink, green, blue, and purple) correspond to the numerical tag per feature and feature type provided in Table S1.

Table S2: Descriptions of feature pairs where the correlation r$\geqslant$0.95, as well as which feature is eliminated from the cluster analysis implemented here and the reasoning.

Feature tag	**Correlated feature tag ($>$ 0.95)**	**Feature to keep**	**Reasoning**
2	3	3	Median more robust metric than mean
5	6	5	Prefer metric for raw waveform than envelope
5	7	5	Get rid of skewness (kurtosis essentially equivalent)
5	8	5	Get rid of skewness (kurtosis essentially equivalent)
6	7	Neither	Reasons above
6	8	Neither	Reasons above
7	8	Neither	Reasons above
10	11	10	More reasonable to keep first 1/3 of the autocorrelation function than that remaining part
25	34	34	25 reports same finding as 34 and for consistency, want to keep all of the same set of features 34 to 37
35	36	Both	Though highly correlated, reasonable variance in the relationship
35	37	Both	Though highly correlated, reasonable variance in the relationship
36	37	Both	Though highly correlated, reasonable variance in the relationship
38	40	38	More meaningful to keep spectral centroid value than width

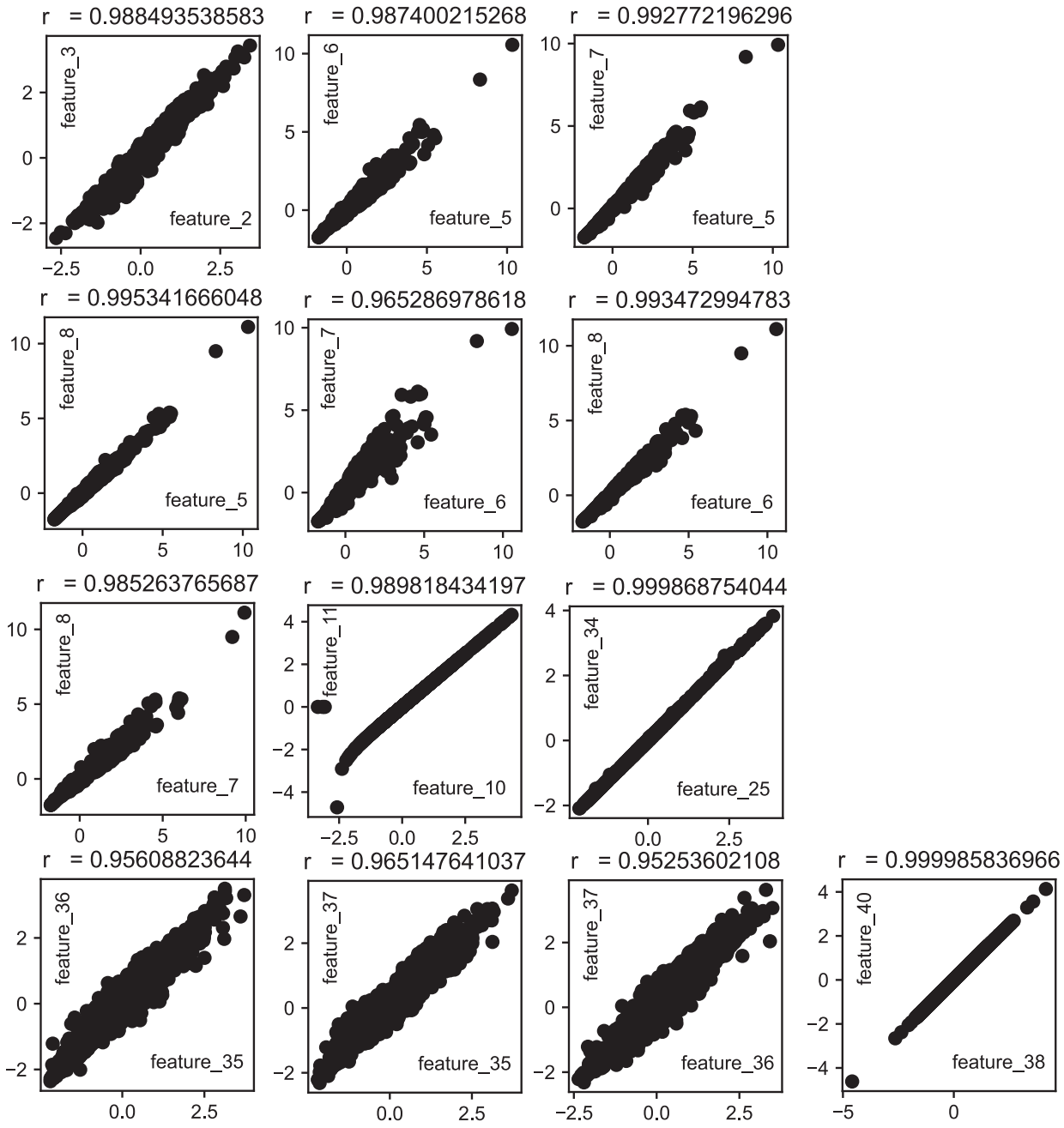

Figure S2. Relationships between each feature pair where the correlation is greater or equal to $r \geqslant 0.95$. Scatter plot depiction contributes to discussion of the similarities or variance between two features' distributions, used to determine which features to remove or keep in the clustering analysis.

S3.3 Quantitative approaches to the number of clusters

The following supplemental section is provided to further the discussion in the main text in Sect. 3.3 on how the number of clusters (k) are prescribed in our k-means++ semi-automated implementation. Below, we explore potential optimized choices of k based on quantitative metrics.

We first consider the Silhouette test, which is a commonly used assessment of cluster separation (Rousseeuw, 1987). For each k from 2 to 29, using an extension of the cluster solutions shown previously up to k=14 (main text, Fig. 5), we show the Silhouette scores weighted by k (Fig. S3a). For our implementation of k-means++, k=14 is a realistic maximum for the WIS; however, here we provide the results up to k=29 for a more extensive quantitative analysis. To interpret the weighted silhouette scores: scores near zero indicate that clusters may be overlapping (i.e. not well-separated) or points have been added to the wrong cluster. Higher scores indicate that the clusters are well-separated. At k=10, we note a moderate local maximum in the weighted silhouette score. Though useful, the Silhouette scores have interpretative limitations since we cannot gain insight into how cluster separation scores vary across the high-dimensional feature set. The evolution of clusters as determined by other estimators, such as Davies-Bouldin score, Elbow score, Calinski-Harabasz index, and Dunn index (Maulik and Bandyopadhyay, 2002), could be a future avenue of investigation.

Therefore, we are motivated to develop a more informative quantitative approach to guide the choice of k. We calculate the similarity of two clusters at a given k, based on the overlap of features within each cluster. We define a 'Similarity Index' akin to that used in the main text, Sect. 3.1.1. However, instead of computing correlation coefficients for each feature pairwise, we quantify the summation of the intersection between each feature distribution of each pair of clusters (referred to as 'histogram overlap'; Smith, 1997). Given clusters A and B, the Similarity Index (U) is defined here as:

$$U(\text{A,B}) = \frac{1}{N}\sum_{j=1}^{N}\sum_{l=1}^{n}\min\left(\frac{A_{jl}}{[\text{count of events in A}]}, \frac{B_{jl}}{[\text{count of events in B}]}\right), \tag{S1}$$

where $n = 100$ is the number of bins, N is the number of features in this analysis (= 30), and the notation A_{jl} and B_{jl} signifies the count of events in cluster A for feature j and bin l. The Similarity Index is scaled by N and the count number of events in each cluster. Therefore, the maximum Similarity Index is 1 when two clusters are entirely similar (i.e. the 30 features are distributed in the same way between a pair of clusters). The minimum Similarity Index is 0 when two clusters are well-separated (i.e. the 30 features are distributed distinctively between a pair of clusters). In order to produce clusters that are well-separated and thus provide unique information, we are looking for a Similarity Index closest to zero.

We apply this metric to the problem of choosing the number of clusters. For each k from 2 to 29, we compute the Similarity Index for all pairs of clusters (Fig. S3b). The number of values comprising the Similarity Index per k equals $k-1$: one pair of clusters to compare for k=2 and two pairs for k=3 and so on. At k=10, we also find a local minimum, in terms of the minimum (bottom 'whisker'), median (white horizontal line), and maximum (top 'whisker') of the range of U. We note two outliers at U=0.7 and U=0.8, which signify two pairs of clusters that are more similar than the other pairs of clusters.

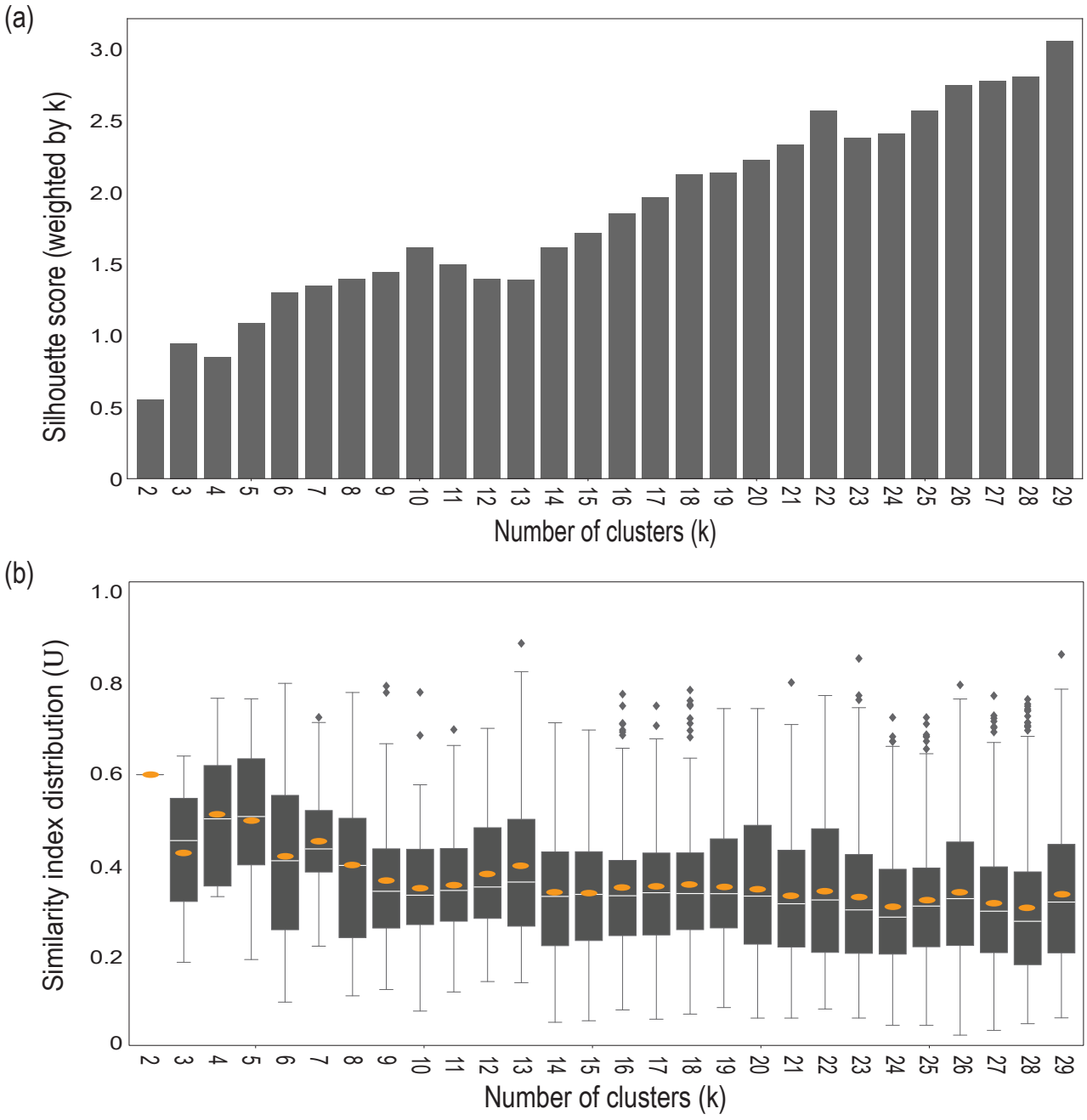

Figure S3. Similarity-based metrics for determining an optimized value of k. We provide results for the: (a) Silhouette test for the k-means++ application on the reference feature dataset, for k = 2 to k = 29. The Silhouette score is computed as: average distance between each point within a cluster subtracted from the average distance between all clusters, divided by the maximum of the two averages. Reported here is the mean Silhouette score per k, weighted by k. (b) Cluster similarity ranges given by the Similarity Index (U) from k=2 to k=29. The range of U is defined as the similarity of event features in each cluster pair permutation per k (defined mathematically in Eq. S1). The symbols on this figure correspond to: orange ellipse, mean; white horizontal bar, median; bottom of rectangle, lower quartile; top of rectangle, upper quartile; bottom whisker, minimum; top whisker, maximum; diamond, outlier. We proceed to perform k-means++ with 10 clusters (k=10).

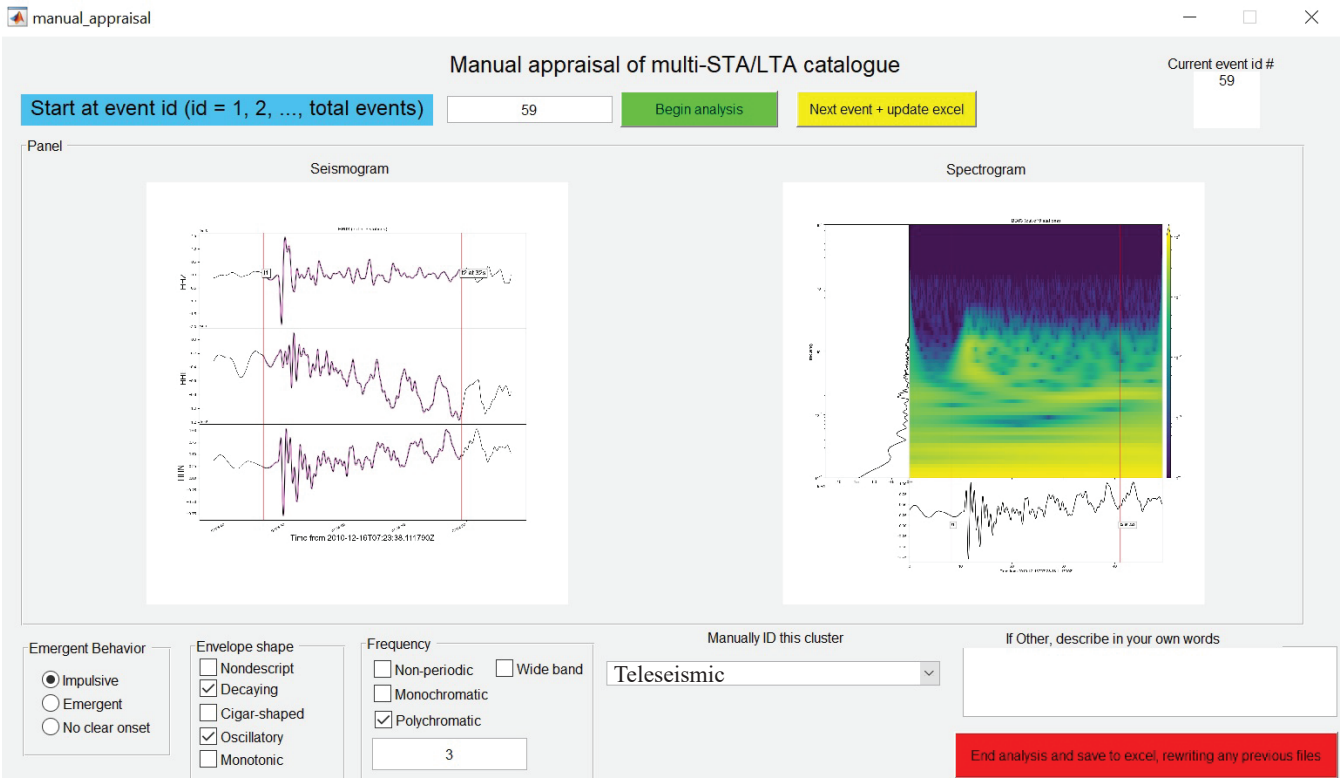

Figure S4. Screenshot of the manual appraisal GUI built and operated through MATLAB. The GUI is used to review the catalogue in terms of the waveform representation and the spectral representation. All fields are required for inputting detail on emergent behavior, envelope shape, frequency description, maximum frequency, and a manual identification of the type of event. Shown as an example is an impulsive event that decays after initial arrival and is oscillatory. The frequency is polychromatic and is at a maximum at 3 Hz. This event is grouped under the cluster of similar fracture-related events. The manual appraisal records user input to a spreadsheet.

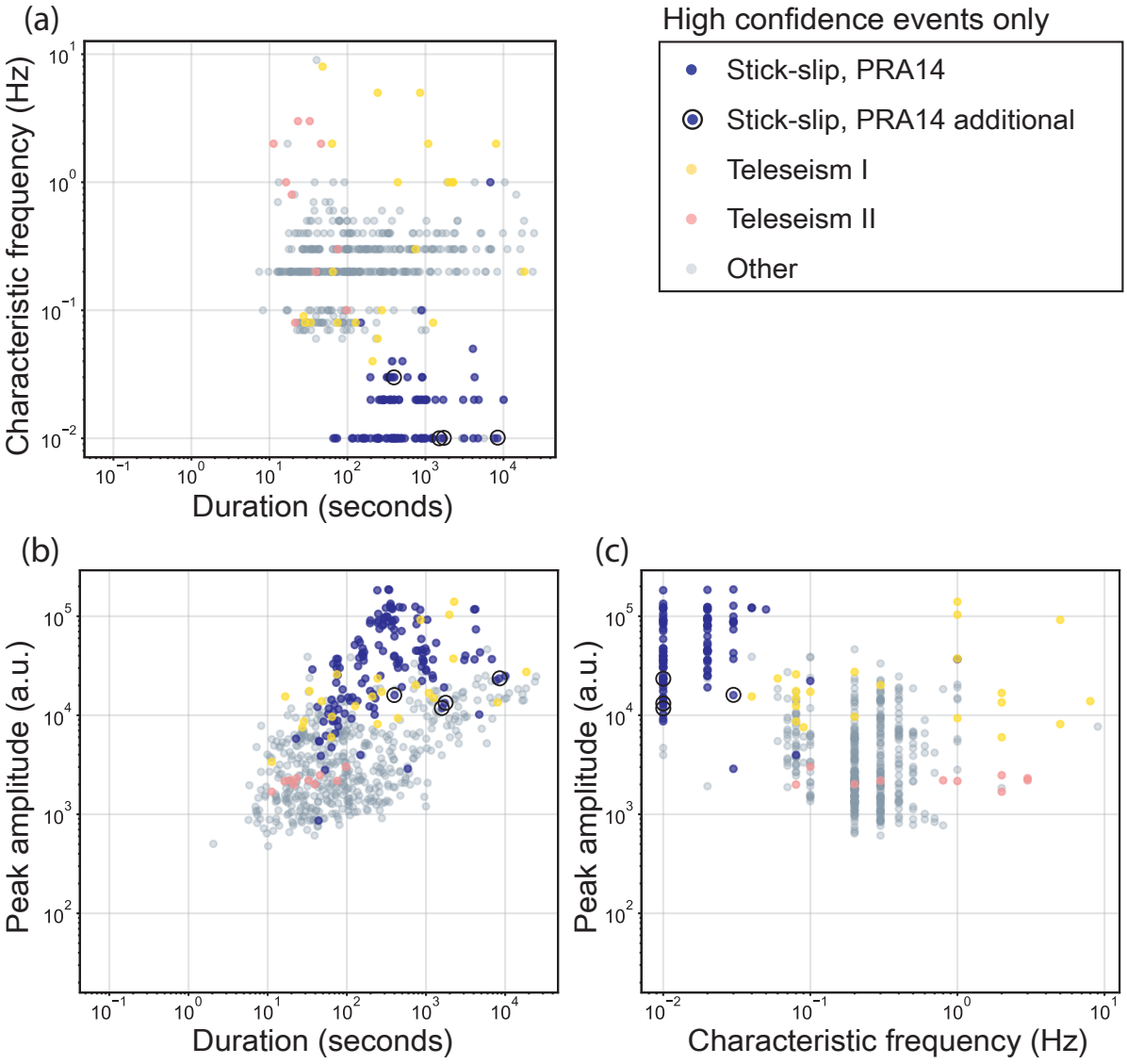

Figure S5. Manual appraisal of the reference event catalogue showing high confidence events only. The features measuring duration (log, seconds) and peak amplitude (log, a.u.) are retrieved from the reference event catalogue and characteristic frequency (log, Hz) is determined from the spectrograms of each event in the manual appraisal. Event types that are identified from the manual appraisal and further validated in subsequent investigation show the natural groupings, or clusters, of events in each bivariate feature pair: (a) duration and characteristic frequency, (b) duration and peak amplitude, and (c) characteristic frequency and peak amplitude.

Table S3: Summary of signal types expected from a cryoseismic deployment. Characteristic frequency, period, and duration are copied from the available literature, reported accurately within the expected orders of magnitude. Comments on waveform structures and expected sources taken from literature as well. 'Potential' refers to a potential for occurrence on the Whillans Ice Stream, i.e. the likelihood of each signal type to be observed from the Whillans Ice Stream deployment discussed in the text (Winberry et al., 2010), including three options: Unlikely, Possible, and Probable. Framework and sources reproduced from Podolskiy and Walter (2016).

Signal type	Freq. (Hz)	Period (s)	Duration	Comment (based on the literature)	Potential
Basal icequakes	100	0.01	0.1s	Impulsive first arrivals. (Helmstetter et al., 2015b)	Probable
Snowquakes	>50	0.02	< 1 s	Emerges with a sharp amplitude then exponential decay. Signals that show fracture in the uppermost snow cover due to thermal stress. (Nishio et al., 1983)	Possible
Hydrofracture	10 – 100 Hz	0.01 – 0.1	1 – 5 s	Impulsive. (Hudson et al., 2020)	Probable
Surface crevassing	10 – 50	0.1 – 0.02	< 1 s	Characterized by a dominant Rayleigh wave and few or no visible P- and S-phase arrivals. (Röösli et al., 2014)	Probable
Ice / serac falls	20	0.05	10 – 100 s	Complex frequency content that is characterized by various sub-events. (Roux et al., 2008)	Unlikely
Subglacial cavity cracking	1 – 100	0.01 – 0.1	1 – 10 s	Impulsive. (Walter et al., 2008)	Unlikely
Crack propagation	12 – 15	0.06 – 0.08	< 1 s	Impulsive arrivals, repeating in multiplets, with rapid decay. (Carmichael et al., 2012)	Possible
Moulin tremor	3 – 11	0.09 – 0.33	6 hours	Cigar-shaped envelope with no clear onsets or phase arrivals. (Röösli et al., 2014)	Possible

Fluid-induced resonance	1 – 10	0.1 – 1	600 s	Long, monochromatic, and harmonic seismic signals related to subglacial lake drainage. (Winberry et al., 2009a)	Possible
Firnquakes	1 – 10	0.1 – 1	< 1 s	Rapid emergence then exponential decay in amplitude. (Lough et al., 2015)	Unlikely
Fracture (thermal bending)	10 – 15	0.06 – 0.1	1 – 5 s	Short, impulsive in the evening. (Lombardi et al., 2019)	Probable
Calving	1 – 3	0.33 – 1	25 – 600 s	Characterized by emergent wave onsets and low frequencies. Range of duration depending on a trigger of rapid succession calving. (Qamar, 1988)	Unlikely
Iceberg resonance	0.5	2	60 – 3600 s	Iceberg harmonic tremor is described as a complex, evolving signal. (MacAyeal et al., 2008)	Unlikely
Local, regional swell	10^{-1}	10	60 – 1200 s	Frequency dependence of arrival times at measurement seismometer based on distance and time from generation. (Hell et al., 2019)	Unlikely
Secondary microseisms	10^{-1} – 10^{0}	5 – 10	1–10 s	Higher amplitude than primary microseisms. Can have a period less than 5 seconds when caused by wind. Cigar shaped. (Cannata et al., 2019)	Possible
Micro-tsunamis	10^{-1}	10 – 30	60 – 1800 s	Impulsive source mechanisms and short durations. (e.g. from iceberg collision; MacAyeal et al., 2009)	Unlikely
Primary microseisms	10^{-1}	10 – 25	10 s	Spectral content equal to the ocean wave frequency. (Cannata et al., 2019; Anthony et al., 2015)	Possible

Glacier basal stick-slip	10^{-2}	30 – 100	$<$ 1200 s	Abrupt, initial rupture, typically composed of 3 phases over 20 – 30 minutes. (Pratt et al., 2014)	Likely
Teleseismic glacial quakes	10^{-2}	35 – 100	10 – 100 s	Characteristic weak high-frequency excitation at the source and long propagation distances. (Nettles and Ekström, 2010)	Unlikely
Infragravity waves	10^{-3} – 10^{-2}	100 – 1000	100 s	Act at an ice shelf front. (Bromirski et al., 2015, 2017)	Unlikely
Seiches	10^{-3} – 10^{-2}	100 – 1000	$>$ 100 s	Seiche frequency depends strongly on basin bathymetry. (Amundson et al., 2012)	Unlikely

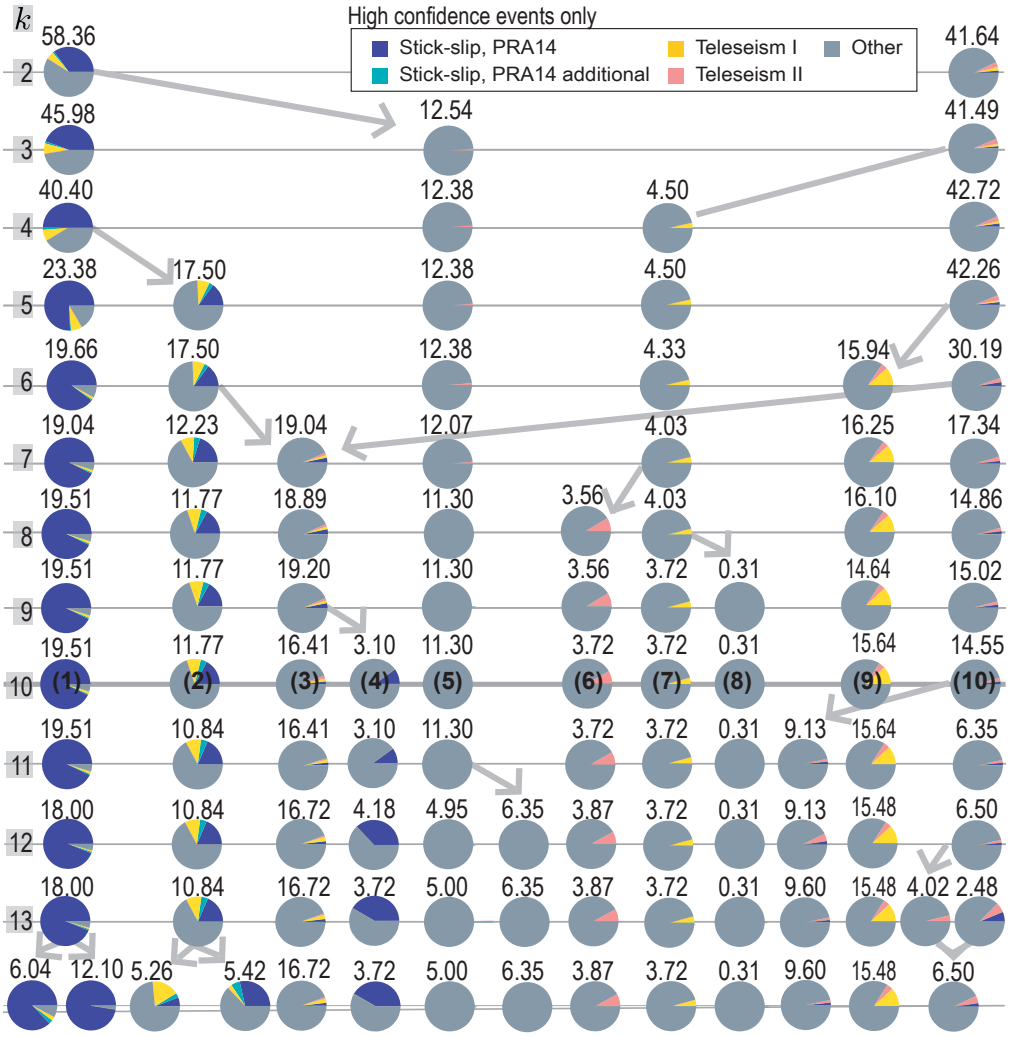

Figure S6. Illustration of how clusters (depicted as circles) evolve in composition from k=2 (top row) to k=14 (bottom row) for high confidence events only. As k increases (top to bottom), each column tracks an individual cluster and arrows indicate when a cluster splits or merges. The heavy grey line at k=10 indicates the preferred value of k, along this row, cluster numbers are counted from left to right (1 to 10) and match those in Table 1 and Figures 6 and 7. The number above each cluster is the % of total events, thereby the numbers across a row sums to 100%. Pie chart segments represent the percentage of events within a cluster, as labelled with an event type during the manual appraisal. Clusters 3, 4, 6, 7, 8, 10 contain events best characterized as noise-types based on the majority labelled as 'Other' and their features (Sect 3). Clusters 1, 2, 5, and 9 contain either labelled events and/or noise that appears related to processes by further analysis. Event types as identified by manual appraisal are shown in the legend; further event types identified by unsupervised learning (Fig. 6) occur in Cluster 5 (events from an icequake swarm, lasting 2 days). The key differences are that the relative size of clusters is variable depending on how many low confidence events are associated with a given cluster. For example, Cluster 3 contains 9.16% of all events but 16.41% of high confidence events only. As another example, Cluster 8 contains 5.71% of all events but 0.31% of high confidence events only. This result emphasizes the level of legitimacy of a cluster's contained events, which can streamline the way by which we investigate and interpret the more noise-dominated clusters in later discussion.

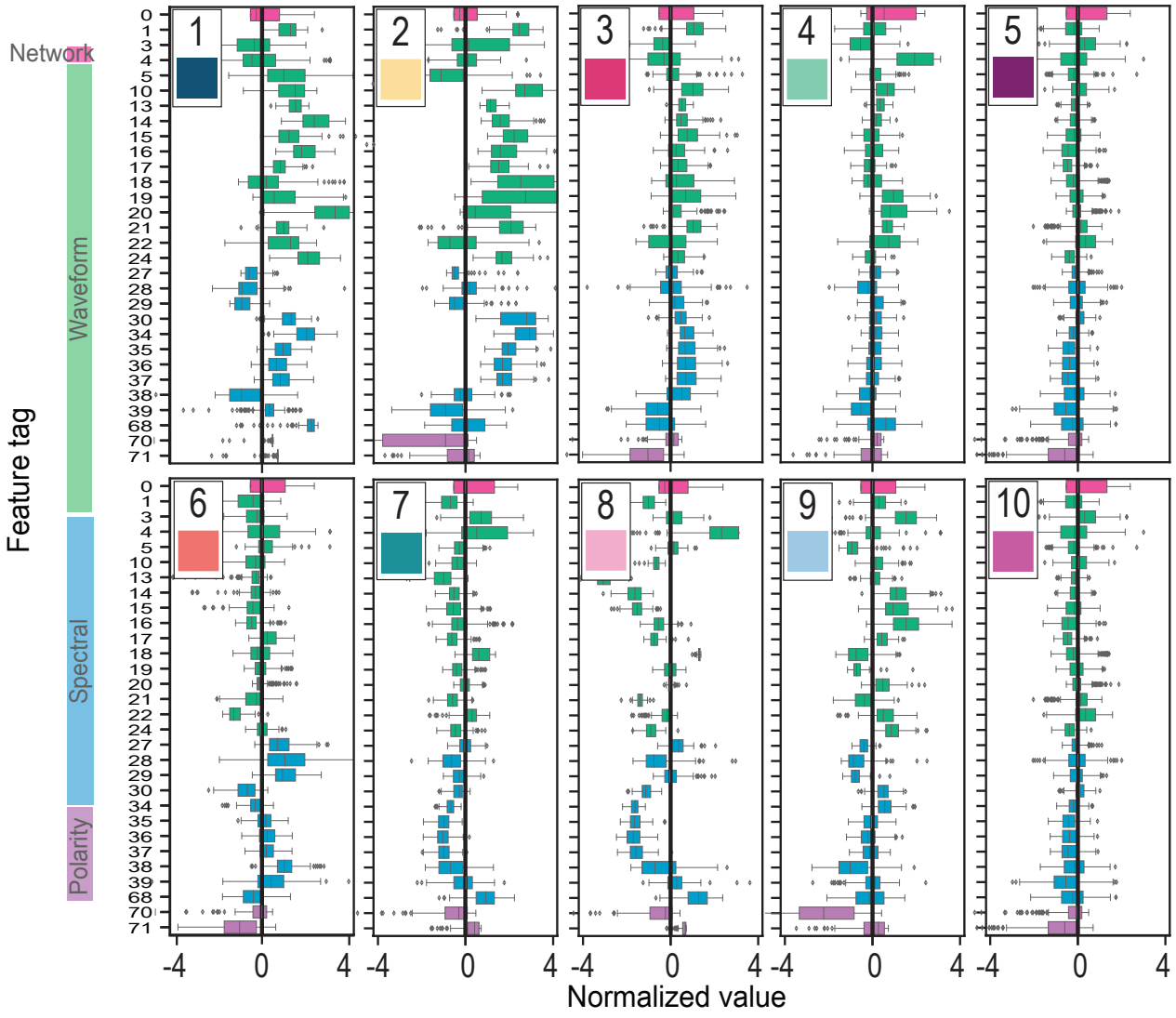

Figure S7. Distributions of features within each cluster for k = 10. Cluster number as assigned in main text is annotated in the top left of every plot. The feature tags and color attributions (top to bottom per figure: pink, green, blue, and purple) correspond to the numerical tag per feature and feature type provided in main text, Table 1. Since each feature is scaled before clustering to have the same median at zero, we can assume that clusters with features at medians farthest from zero are best differentiated from other clusters by those more extreme features. Therefore, we report the six features per cluster with the most extreme median values. This type of analysis is useful for comparing two clusters. For example, Clusters 1 and 2 are both assigned stick-slip events, so it is of interest to understand why all stick-slip events are not characteristic to one cluster. The feature distributions within each cluster may be informative, such as Cluster 1 being characterized by shorter event lengths (Fig. S5) whereas Cluster 2 is differentiated most from other clusters by longer event lengths.

Table S4: Reference for the spatial attribution discussed in main text, Table 1, and used to compile Fig. 6 in main text. Provided is the percentage of each cluster's seismic events that are included in each cluster as detected by each seismometer.

Cluster	1	2	3	4	5	6	7	8	9	10
BB01	13.76	8.00	10.59	**6.47**	**13.06**	4.59	**9.29**	3.65	10.59	20.00
BB03	**30.02**	12.11	8.47	4.36	5.81	3.39	7.02	2.18	**14.53**	12.11
BB04	**45.26**	13.33	4.56	0.70	1.40	1.05	2.11	0.00	**24.91**	6.67
BB06	**28.40**	**18.93**	9.05	**7.00**	4.12	2.88	5.76	1.65	10.29	11.93
BB07	9.52	5.93	9.70	**5.75**	12.67	**9.70**	**8.36**	**4.76**	8.45	**25.16**
BB08	10.32	8.88	**11.17**	5.01	11.32	5.73	8.17	3.72	10.03	**25.64**
BB10	13.15	5.80	**12.11**	4.55	4.14	**9.52**	**8.39**	**4.76**	8.49	**29.09**
BB11	18.41	**13.52**	8.86	2.56	5.83	8.16	6.53	3.73	**16.55**	15.85
BB12	11.45	5.73	10.55	4.27	**13.64**	**11.82**	7.09	**5.45**	6.27	23.73
BB13	8.93	8.05	**10.82**	2.77	6.67	**10.82**	**9.69**	**5.41**	9.56	**27.30**
BB14	**42.92**	**16.81**	6.64	4.87	3.10	1.33	3.10	0.88	10.62	9.73
BB15	17.27	8.49	10.50	**7.63**	**19.71**	3.02	5.90	1.87	10.36	15.25
BB16	12.84	11.39	10.49	3.07	**20.25**	3.98	6.33	2.89	11.39	17.36
BB17	20.91	**17.27**	**12.73**	4.55	5.45	3.64	4.24	2.42	**18.79**	10.00

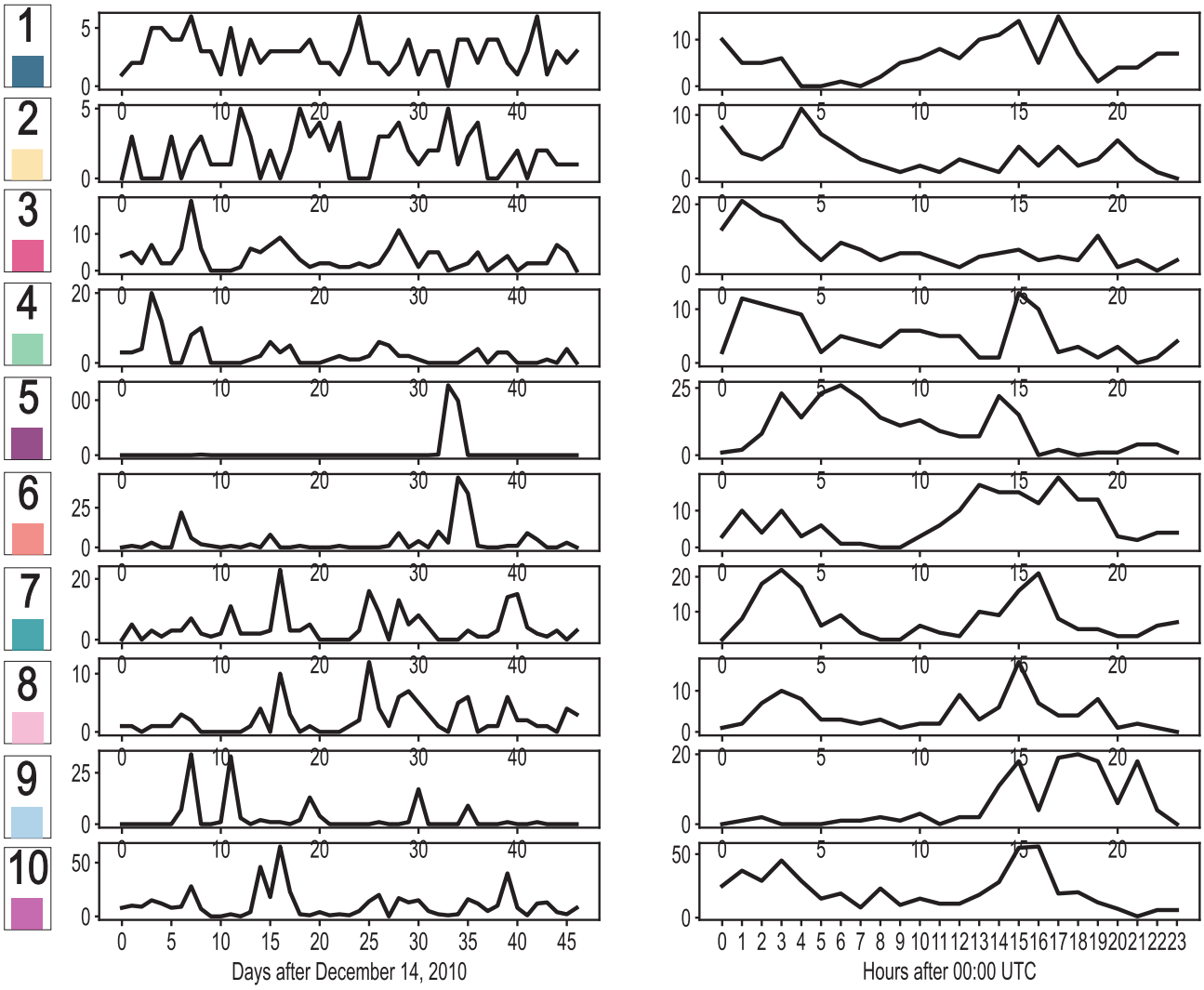

Figure S8. Reference for the temporal attribution discussed in main text, Table 1, and shown synthesized in main text, Fig. 6. Provided are the individual time series of each cluster's seismic event count per day (left column) and per hour (right column).

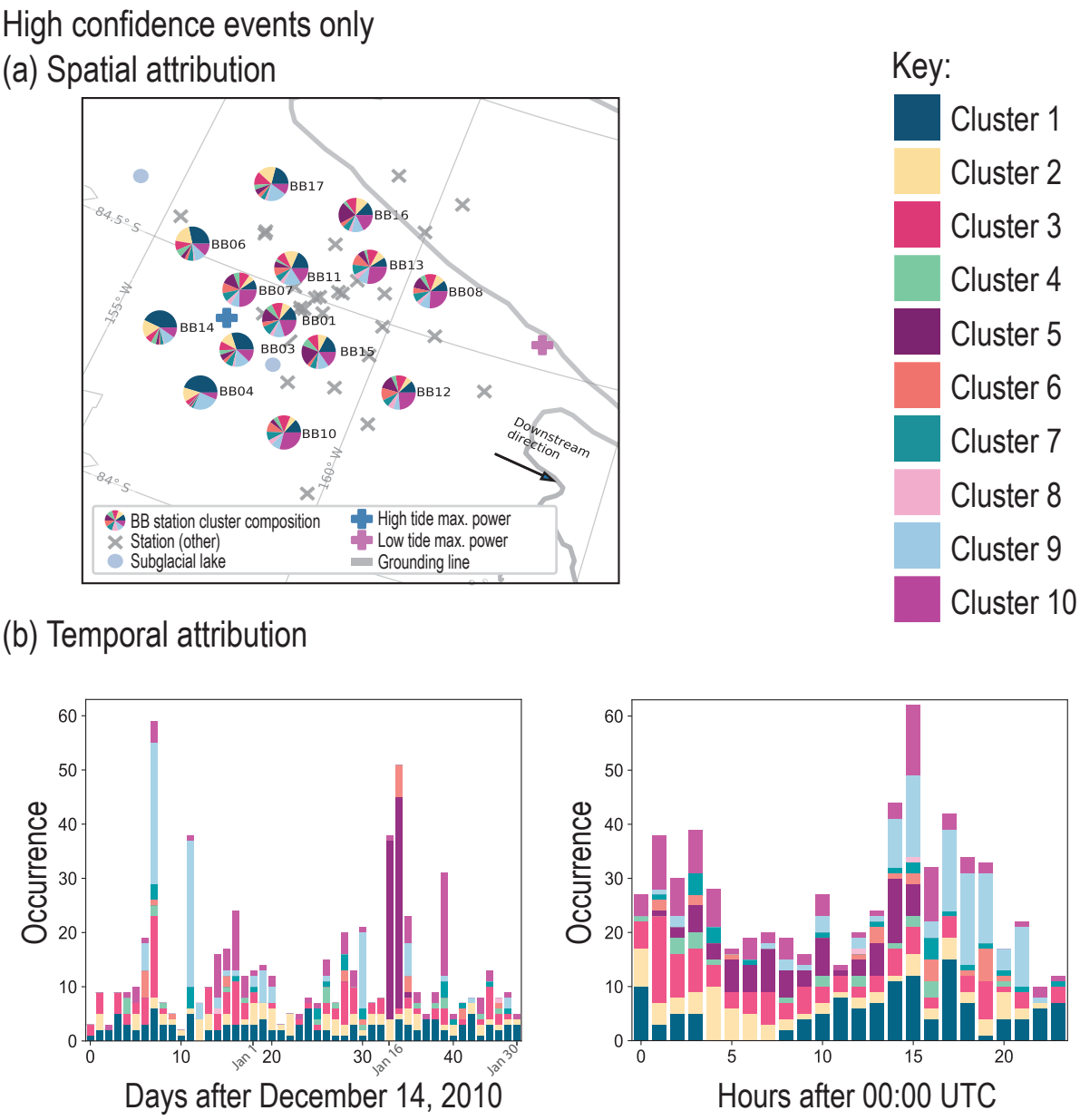

Figure S9. The (a) spatial and (b) temporal attribution of clusters for k=10 showing high confidence events only. The spatial attribution pie chart segment colors corresponds to the numerical cluster assignments provided in the key. The temporal attribution is provided as a daily occurrence for days after December 14, 2010, with annotated reference dates Jan 1, Jan 16, and Jan 30, and an hourly occurrence for hours after 00:00 UTC, where solar noon falls in the time zone of 22:00 UTC. In conjunction, both attributions are used to better characterize the clusters for k=10. The results of the spatio-temporal analysis are synthesized in Table 1. A breakdown for the spatial attribution and temporal attribution is provided in the Supplementary Materials (Table S4 and Fig. S8, respectively). Colors were chosen for clarity between separate classes (Glynn and Naylor, 2021, Ordnance Survey).

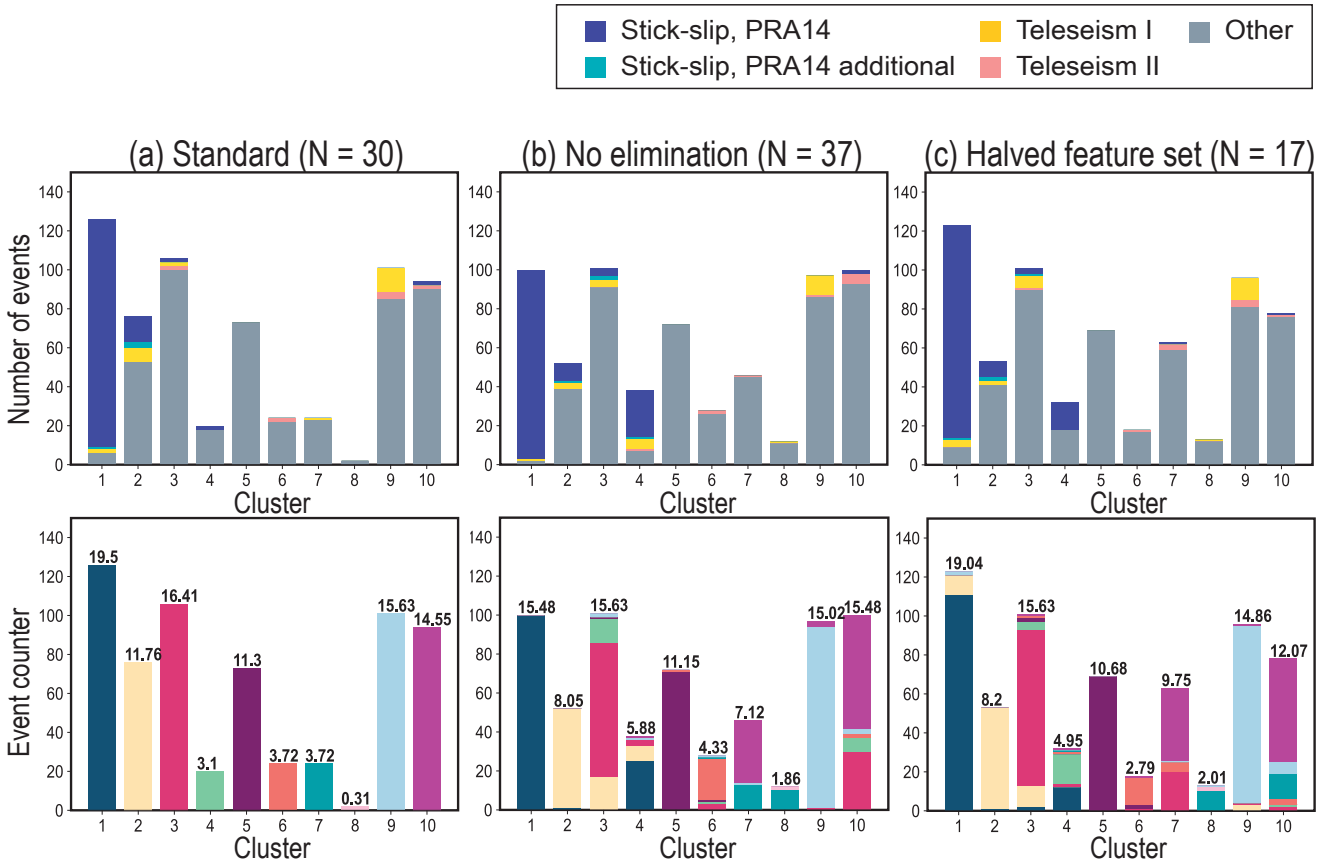

Figure S10. Stability of cluster results compared with the standard procedure showing high confidence events only. From left to right columns, we show (a) the standard set of features after removal of selected members of the feature pairs with r⩾0.95, (b) the results of clustering with no features eliminated, and (c) the results with a halved feature set. The top row provides the percentage composition of each cluster 1–10 as determined from the manual appraisal. The bottom row provides the number (and percentage) of events that are grouped in each cluster. The order and labelling of the clusters in the (b) and (c) columns is manually decided by a comparative method that matches clusters approximately one-to-one for each application, when possible. The colors within each cluster in the bottom row signify where the contents of the clusters resulting from applying the algorithm to the standard feature are placed in the two comparison applications of the algorithm.

The clustering procedure has enabled an informative analysis of the clusters found with semi-supervised learning, described in detail in this section. The significance of the sign (i.e. positive or negative) of each discriminant feature per cluster (Table S5) is used here to describe the event types represented in each cluster. We review that the term 'platykurtic' is used to describe a distribution with less kurtosis than the normal distribution and is more typical for higher amplitude events (i.e. are of high strength) (Hibert et al., 2014).

Table S5: Explanations for most discriminant feature as most negative or most positive in a distribution. Useful for explanation of cluster seismic signal context in main text (Sect. 4).

Feature	Negative	Positive	Citation
0	N/A	N/A	
1	Short duration	Long duration	
3	Low ratio signifies high strength event	High ratio signifies low strength event	Hibert et al. (2014)
4	More impulsive	Slow emergence	Hibert et al. (2014)
5	Flatter amplitude distribution (platykurtic) typical for higher strength events	Sharper distribution than the normal (leptokurtic) are more common for ambient noise	Hibert et al. (2014)
10	Higher signal to noise ratios	Tremor-like	Langer et al. (2006)
13	Low energy	High energy	
14	Low energy	High energy	
15	Low energy	High energy	
16	Low energy	High energy	
17	Low energy	High energy	
18	Low energy in flatter distribution	High energy in sharper distribution	
19	Low energy in flatter distribution	High energy in sharper distribution	
20	Low energy in flatter distribution	High energy in sharper distribution	
21	Low energy in flatter distribution	High energy in sharper distribution	
22	Low energy in flatter distribution	High energy in sharper distribution	
24	Low frequency content	High frequency content	
27	Low frequency of $<25\%$ power	High frequency of $<25\%$ power	
28	Low frequency of median power	High frequency of median power	
29	Low frequency content	High frequency content	
30	Low variance in frequency content	High variance in frequency content	
34	Low energy in frequency band	High energy in frequency band	
35	Low energy in frequency band	High energy in frequency band	
36	Low energy in frequency band	High energy in frequency band	
37	Low energy in frequency band	High energy in frequency band	
38	Low weighted mean of the frequencies	High weighted mean of the frequencies	
39	Narrow fracture	Wide fracture	Sayers and Calvez (2010)
68	No preferred direction	Linear polarization	Hammer et al. (2012)
70	Propagating more from horizontal plane	Propogating more from vertical plane	Hammer et al. (2012)

71	No preferred direction	Polarization in plane	Hammer et al. (2012)

Table S6: Cluster attribution for k = 10. Descriptions of the active glacier process or noise events and how the cluster attribution is determined, such as by unsupervised learning (UL).

Cluster	Process event name (if distinct)	Noise event description	Process interpretation (proposed)	Further remarks	Comment, including processes not likely
1	Stick-slip		High-energy, source near sticky spot.		Stick-slip events matched to previous studies.
2	Stick-slip, Teleseismic		Long, high-energy.		Stick-slip events matched to previous studies, some newly identified by UL. Teleseismic events verified by global catalogues.
3		High-energy, long, tremor-like	External wavefield?		Identified by UL
4		High-energy, emergent, tremor-like	External wavefield?		Identified by UL
5	Event swarm		External swarm of high-freq. fractures from Jan. 16 to 17.	Potential cause can be melt on RIS. Similar Jan. 10–16, 2016 RIS icequake swarm attributed to melt-driven fracture (Chaput et al., 2018; Jenkins et al., 2021a).	Identified by UL. Swell and ocean infragravity wave causes unlikely due to limited time span.
6		Low-energy, high-freq. content	External wavefield?	Temporal correlation with event swarm (Cluster 5).	Identified by UL.
7		Low-energy	External wavefield?		Identified by UL.
8		Low-energy, emergent	External wavefield?		Identified by UL.
9	Teleseismic		Global earthquakes and other high energy events.	Other high energy events occur in the 14 to 21 UTC window. Potential sources are external wavefield fractures.	Identified in manual appraisal, also identified by UL.
10		Low-energy	External wavefield?	Cluster evolution from k=2 to k=14 indicates high variability in the character of events.	Identified by UL.

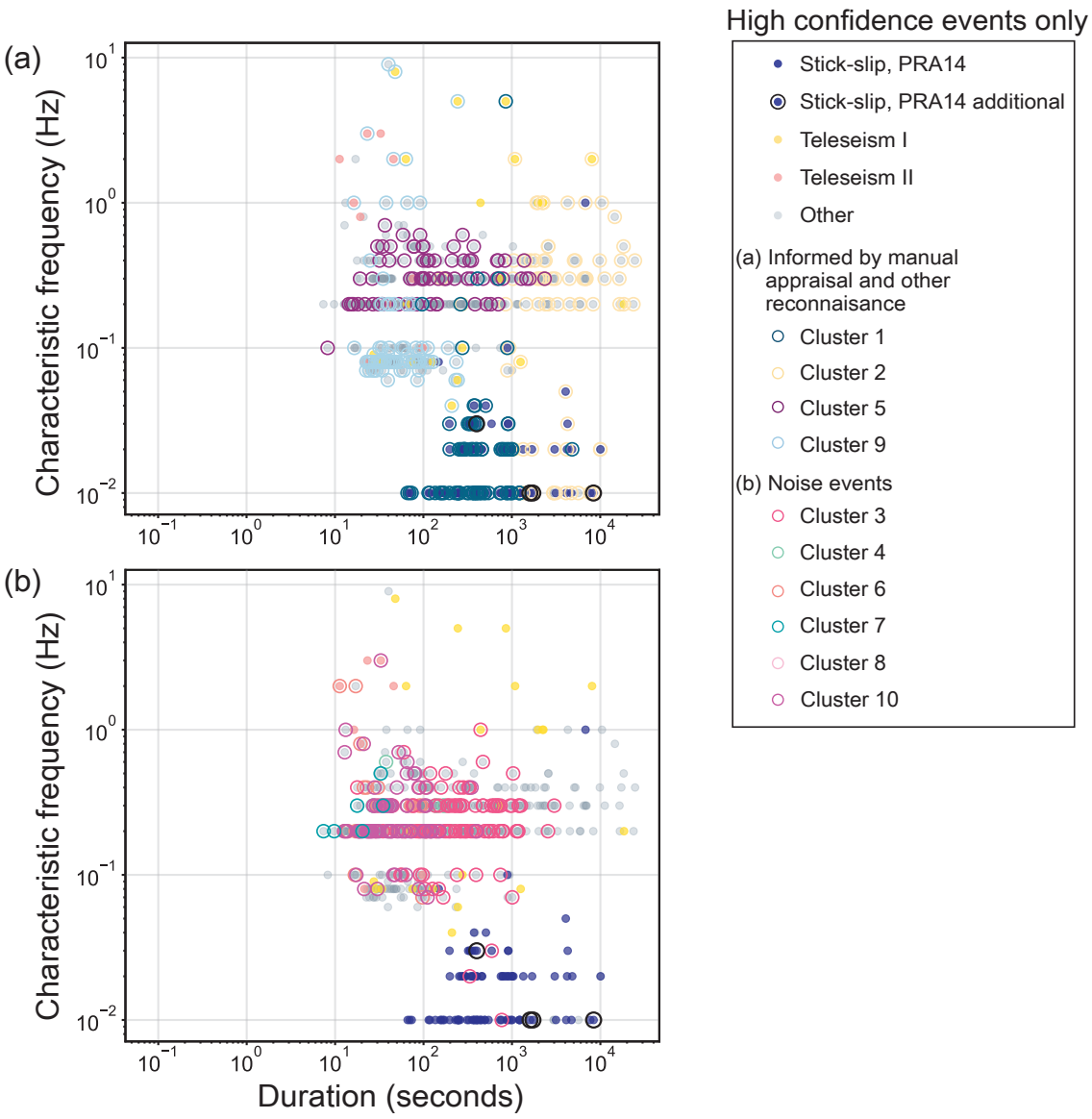

Figure S11. Synthesis of the Whillans Ice Stream duration and frequency relationships by manually identified event types and unsupervised learning clusters showing high confidence events only. For the manually identified events, as labelled from the thesis research, are designated by filled circles. The clusters are shown in the two plots as (a) Clusters informed by manual appraisal and other reconnaisance, including Cluster 1 (stick-slip), Cluster 2 (stick-slip), Cluster 5 (potentially icequake swarm), and Cluster 9 (teleseismic and potentially external fracture-related), (b) Clusters likely pertaining to noise-type events, including Clusters 3, 4, 6, 7, and 8. Some event types can be concealed by other symbols; the events of type 'Other' and other manually identified events are arranged in the background, such that the unsupervised learning result is in the foreground.